Title

Investigating the minimum scan parameters required to generate free-breathing motion artefact-free fast-helical CT

Journal

British Journal of Radiology, 91(1082)

ISSN

0007-1285

Authors

Thomas, David H
Tan, Jun
Neylon, Jack
et al.

Publication Date

2018-02-01

DOI

10.1259/bjr.20170597

Peer reviewed

BJR

https://doi.org/10.1259/bjr.20170597

Received: 15 August 2017 | Revised: 30 October 2017 | Accepted: 31 October 2017

Cite this article as:
Thomas DH, Tan J, Neylon J, Dou T, O'Connell D, McNitt-Gray M, et al. Investigating the minimum scan parameters required to generate free-breathing motion artefact-free fast-helical CT. *Br J Radiol* 2018; **91**: 20170597.

FULL PAPER

Investigating the minimum scan parameters required to generate free-breathing motion artefact-free fast-helical CT

[1]DAVID H THOMAS, PhD, [2]JUN TAN, PhD, [3]JACK NEYLON, PhD, [3]TAI DOU, PhD, [3]DYLAN O'CONNELL, MS, [4]MICHAEL MCNITT-GRAY, PhD, [3]PERCY LEE, MD, [3]JAMES LAMB, PhD and [3]DANIEL A LOW, PhD

[1]Department of Radiation Oncology, University of Colorado School of Medicine, Aurora, CO, USA
[2]Department of Radiation Oncology, University of Texas Southwestern Medical Center, Dallas, TX, USA
[3]Department of Radiation Oncology, University of California, Los Angeles, California, CA, USA
[4]Department of Radiological Sciences, University of California, California, CA, USA

Address correspondence to: Mr David H Thomas
E-mail: *david.h.thomas@ucdenver.edu*

Objective: A recently proposed "5DCT" protocol uses deformable registration of free-breathing fast-helical CT scans to generate a breathing motion model. In order to allow accurate registration, free-breathing images are required to be free of doubling-artefacts, which arise when tissue motion is greater than scan speed.
Methods: Using a unique set of digital phantoms based on patient data and verified with a motion phantom, this work identifies the minimum scanner parameters required to successfully generate free-breathing artefact-free fast-helical scans. A motion phantom and 5 patients were imaged 25 times under free-breathing conditions in alternating directions with a 64-slice CT scanner employing a low-dose fast-helical protocol. A series of high temporal resolution (0.1s) 5DCT scan data sets was generated in each case. A simulated CT scanner was used to "image" each free-breathing data set. Various CT scanner detector widths and rotation times were simulated, and verified using the motion phantom results. Motion-induced artefacts were quantified in patient images using structural similarity maps to determine the similarity between axial slices.
Results: Increasing amounts of motion-induced artefacts were observed with increasing rotation times >0.2 s for 16 mm detector configuration.
Conclusion: The current generation of 16-slice CT scanners, which are present in the majority of Radiation Oncology departments, are not capable of generating free-breathing sorting artefact-free images required for 5DCT.
Advances in knowledge: A recently proposed "5DCT" protocol uses deformable registration of free-breathing fast-helical CT scans to generate a breathing motion model. In order to allow accurate registration, free-breathing images are required to be free of doubling-artefacts, which arise when tissue motion is greater than scan speed. The results suggest that the current generation of 16-slice CT scanners, present in the majority of Radiation Oncology departments, are not capable of generating the free-breathing images required for 5DCT.

INTRODUCTION

Respiration-induced motion is a considerable source of uncertainty in radiotherapy treatment planning,[1,2] and has the potential to lead to substantial dose delivery errors if not properly accounted for.[3] Respiratory-gated four dimensional CT (4D-CT) offers spatial and temporal information on tumour motion and has become indispensable for the highly conformal treatment of lung tumours.[2] Current commercial clinical 4D-CT images are typically acquired using either low-pitch helical[4] or ciné acquisition sequences.[5,6] Scans are combined with simultaneous breathing surrogate measurements to retrospectively group acquired projections (helical protocols) or images (cine protocols) according to breathing phase, using either amplitude-based or phase-based sorting.[7–10] These techniques perform well under conditions of regular breathing with a consistent breathing depth, but image artefacts arise under conditions of irregular breathing,[11] leading to systematic errors in tumour volume and centre of mass measurements.[12]

We recently published a novel sorting artefact-free 4D-CT technique that exploits repeated standard fast-helical acquisition, a simultaneous breathing surrogate measurement, deformable image registration (DIR) and a breathing motion model.[13] The technique is termed "5DCT", named

Table 1. Typical 16-slice CT scanner parameters

Gantry	GE Light Speed 16	GE Bright Speed 16	Phillips Brilliance Big Bore 16	Toshiba Aquilion 16	Siemens Sensation 16
Nominal slice widths (mm)	0.6–10	0.6–24	0.6–24	0.5–8	0.63–10
Range of gantry rotation times (s)	0.5–4	0.5–4	0.24–4	0.4–3	0.3–1.5

after the five parameters of the motion model; the three spatial dimensions, breathing amplitude and phase. The technique uses a repeated fast helical CT protocol, with multiple scans acquired to sample the breathing cycle. Each scan is performed during free breathing. Owing to the relative motion of the tissue and the scanner during the acquisition process, the 25 free-breathing images do not correspond to any single breathing phase. As the speed of the helical scan is much greater than the tissue motion, each individual axial slice can be considered to be acquired at a single static respiratory phase and thus contain minimal blurring artefacts. DIR and a breathing motion model is used to relate tissue motion to breathing amplitude and phase in order to generate low-noise sorting artefact-free images. The technique has been applied successfully using a 64-slice scanner (38.4-mm detector configuration, pitch of 1.2, rotation time of 0.24 s). Owing to the relative motion of the tissue and the scanner during the acquisition process, free-breathing images did not correspond to any single breathing phase. As the CT scanning speed (defined as the couch velocity) was much faster than tissue motion, all tissues were accurately imaged during free-breathing and the images are free of doubling artefacts.

However, CT simulation for radiotherapy treatment planning is most commonly performed on 16-slice CT scanners. Typical scan parameters are shown in Table 1. Optimal scan parameters, including pitch, mAs, detector configuration etc. may vary dependent on the specific application; *e.g.* a stereotactic treatment of small lung nodules may require a thin slice CT, or use of i.v. contrast may require a specific CT acquisition timing protocol. A wide range of scan parameters are often available, and will vary based on the specific technology available on the scanner; *e.g.* a "*Z*-flying focal spot" is available on Siemen's scanners effectively doubles the samples along the axial direction. An operator's choice for a scanning parameter such as pitch is often dependent on other parameters, and limited by the maximum table speed that the scanner allows. As such, a wide-ranging investigation of all scanning parameters is beyond the scope of this work, and we have chosen to focus on the effect of varying the table motion per rotation (Table 2), which is determined by a combination of other CT scan parameters. If the table motion per rotation is on the order of the tissue motion, the tissue position and shape can be heavily distorted (Figure 1b). Significant breathing motion-induced doubling artefacts have been observed when applying the technique on a single patient using a slower scanner (12 mm detector configuration, 0.44 s rotation time, pitch of 1.18). Example images of 64- and 16-slice data are shown in Figure 1, with doubling artefacts clearly present at the diaphragm in patient 2 (16 slice, artifacts circled). Chen et al[11] summarized motion artefacts in detail using a single slice scanner, performing a phantom study outlining the types of artefacts which may arise for differing conditions. They showed that object shapes can be significantly distorted and the geometric centre of the object can be shifted by almost the full extent of the motion. Tanyi et al[14] similarly investigated artefacts that arise in single and 4-slice acquisition as a function of specific scan parameters, using an anthropomorphic phantom to study the impact of 3D target motion. They showed that motion can result in aliased overestimation of the target volume and misrepresentation of centroid location. Chen et al[11] extended the parameter space of their study using approximate results obtained through a simplified computer simulation of CT scanning of a sphere. However, as they state in the paper "No attempt was made to truly simulate the complex process of collecting ray projections through a [moving] object and performing a CT reconstruction". Our current study was designed to do this and to determine the range imaging parameters that would be able to support the new 5DCT protocol.

The presence of free-breathing motion artefacts at slow scan speeds is known. In this paper, we present the results from a simulation of free-breathing fast-helical CT scanning to quantify the scan parameters which cause artefacts to be present. We used a published 5DCT protocol to generate a digital free-breathing patient data set (five patients), and used a variety of simplified simulated CT scanner geometries to identify the scan parameters required to produce artefact-free free-breathing images. The simulation results were verified with a physical motion phantom. These initial results suggest that the current generation of 16-slice CT scanners, which are present in the majority of Radiation Oncology departments, are not capable of generating the artefact-free free-breathing fast-helical images required to support the 5DCT protocol.

METHODS AND MATERIALS

Simulation

Figure 1a,b shows examples of 16- and 64-slice free-breathing helical CT's. Figure 1c shows the workflow of the scanner

Table 2. Scanner imaging parameters used to acquire measured images

Slices	Scanner	Detector configuration	Pitch	Rotation time	Table movement per rotation
16	Philips Brilliance Big Bore	12 mm	1.2	0.44s	14.4 mm
64	Siemens Definition Flash	38.4 mm	1.18	0.24s	45.3 mm

Figure 1. Examples of free-breathing fast-helical scans for two patients using (a) 64-slice Siemens Definition Flash (Siemens Healthcare, Forchheim, Germany) (approximately half a breath taken during a 1.6 s acquisition) and (b) 16-slice Philips Brilliance Big Bore (Philips Healthcare Systems, Andover, MA, USA) (approximately one and a half breaths taken during a 3.8 s acquisition). The breathing trajectories during the scan acquisition are shown on the left. Artefacts (encircled) are evident in (b) at peak velocity. (c) Workflow of the scanner simulation.

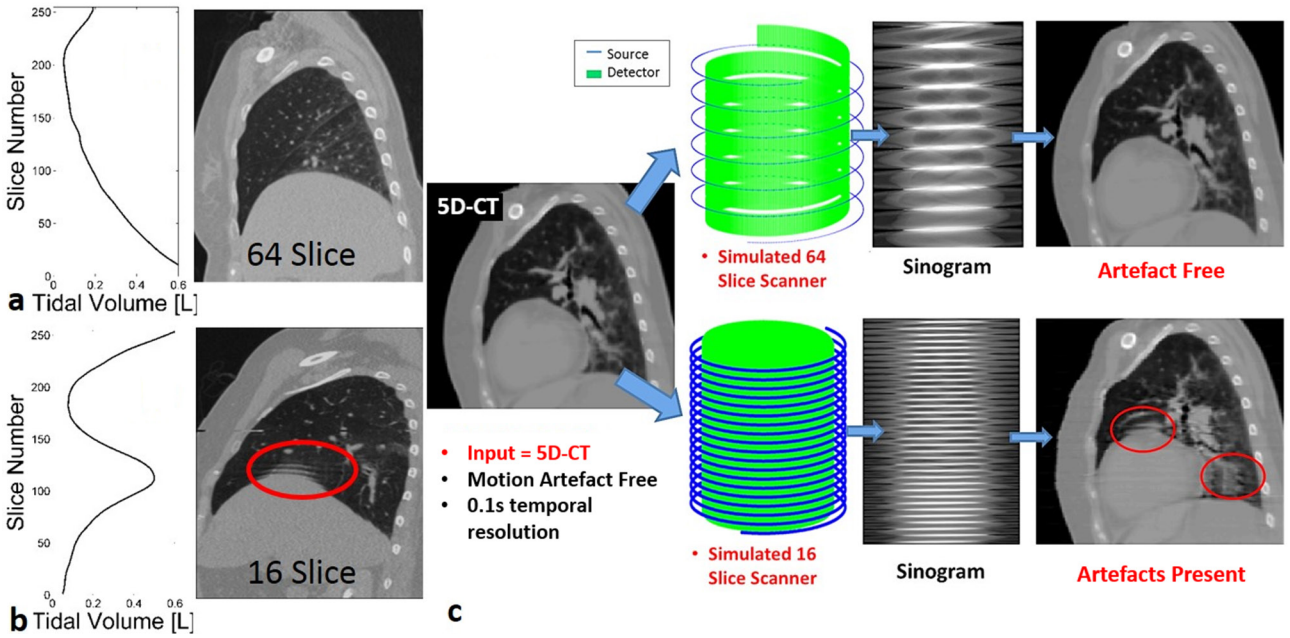

simulation, with examples of the 5DCT image used as input, the helical geometry used to acquire projections, the 3D sinograms generated from simulated forward projections and finally the reconstructed image. Each of these steps is described below.

Input

In order to simulate a range of scan parameters, computer simulations of free-breathing helical CT data using 16 and 64 mm detector configuration were generated. In the case of the phantom data, image data were generated by translating the phantom position in a static CT image and digitally casting projections through the phantom as its motion was simulated

For the patient data, the inputs to the simulation were 5DCT data,[13] (described further below). Under an IRB-approved protocol, five patients were imaged using a 64-slice CT scanner (Siemens Definition Flash). 25 successive low-dose scans were performed in alternating directions, under free-breathing conditions. Total imaging time ranged from 120 to 160 s, delivering approximately equivalent dose to a conventional low-pitch-helical 4D-CT protocol. Each CT scan was acquired at an arbitrary breathing phase, and an abdominal bellows system (Philips Medical Systems) was used to provide a breathing cycle surrogate. For each patient, the first acquired image was arbitrarily chosen as the reference image. This image was segmented using a region-growing tool in a commercial software package (MIM v. 5.6, MIM Software, Cleveland, OH) to isolate the lungs and main-stem bronchi. DIR was implemented on the segmented lung images using an open source software package, "Elastix" (Erasmus Medical Center, Biomedical Imaging Group, Rotterdam). A B-spline registration algorithm was used to register the reference image to the subsequent 24 segmented images (the target images). Accurate registration of the shear motion between the lungs and chest wall was achieved by implementing a linear combination of multiple B-Spline registrations and ensuring that tissue displacement was continuous in the direction normal to the sliding interfaces, using the lung contour to define the interface.[15] The 5D breathing motion model proposed by Low et al[16] was used, implemented using fast helical CT and analysis as described in detail in by Thomas et al[13] The registered voxel locations were used to determine the motion model parameters for each voxel, which related tissue motion, calculated from the DIR, to breathing amplitude and rate as measured with a breathing surrogate. The motion model parameters were used to generate breathing-gated CT scans. Measured patient breathing waveforms were used as an input to the motion model to calculate deformation vector fields, which were in turn used to deform a reference image to generate an image at each required time point. Images were generated at a frame rate of 10 Hz.

To analyse the worst case scenario and maximize the potential for artefacts to be present within the reconstructed image, the equivalent of the scan start times were synchronized to ensure the diaphragm was at its maximum velocity as it was scanned, as was the case for the image shown in Figure 1b.

CT forward projections

Helical CT combines X-ray source rotation with continuous patient translation (along the rotation axis). Consecutive

projections at consecutive angles are measured as the patient is moved axially.

Two simplified CT scanners with a detector configuration of 16 and 64 mm were simulated. The detector configuration of the 16-mm scanner was chosen to match the fastest scan time for a 16-slice scanner, as shown in Table 1. Helical forward projections representative of those shown in Table 2 were calculated with scanner rotation times varying from 0.1 to 2.0 s per rotation, in timesteps of 0.1 s. Simulation of forward X-ray projections with helical cone-beam geometry was implemented with an Nvidia GeForce GTX 680 (NVIDIA Corporation, Santa Clara, CA), to generate the three dimensional sinograms. Forward projection using 800 projections per rotation was performed on 1–5 min of image data, depending on the image size and rotation time.

Image reconstruction

A fast graphics processor unit (GPU) implementation of Katsevich's exact reconstruction algorithm[17] using the methods described by Tan et al[18] was used to reconstruct the CT images. Reconstruction of a typical image data set (512 × 512 × 256 voxels) required approximately 60 s using an NVIDIA GPU.

Artefact detection

The locations of tissues in free-breathing images were accurately represented, but owing to the artefacts which arise from the interplay between the object and scan speeds, the tissue motion was difficult to measure using image registration. Image quality metrics are usually classified according to the availability of an original, distortion-free image for comparison, a "ground-truth".[19] The motion artefacts present in the reconstructed images here were difficult to quantify, as there was no artefact-free "ground-truth" available to compare against; free-breathing images were deformed with regard to a static reference image, regardless of the presence of artefacts, so a "no-reference" or "blind" method was, therefore, required to quantify the severity of motion artefacts.

Patient images were first visually inspected for motion-induced artefacts. We made the distinction here between "blurring"—where a vessel appeared larger than in reality when its motion was on the order of the scan speed, and other motion-induced artefacts, such as doubling—where a vessel appeared more than once within an image, typical of the case when its motion was greater than the scan speed. While both of these artefacts arose from the interplay between the object and scan speeds, the doubling artefacts have been shown to cause a greater degradation to image registration accuracy, when compared with ground truth images.[20]

Artefacts in the reconstructed images were assessed using structural similarity metric (SSM)[19] to determine the similarity between axial slices. The image volumes were segmented using a semi-automatic region-growing tool to isolate the lungs and mainstem bronchi (MIM v. 5.6; MIM Software, Cleveland, OH), and regions outside these contours set to the Hounsfield unit of air (−1000). The local structural similarity of each 10 × 10 × 10 voxel block of an axial slice of the segmented images was compared with that of the next five axial slices, in the direction of the scan and a mean value (SSM) calculated to determine the amount of doubling of vessels. The amount of artefacts present in the image was quantified by calculating the percentage of the image with SSM above a threshold. This threshold was determined by visually identifying artefacts in the images.

Data acquisition

Phantom data

A 30-cm long natural sponge was employed as the imaged phantom. The sponge contained an array of connective structures that formed a complex 3D lattice. The sponge was attached to a one dimensional translational stage that was moved in a pattern based on measured patient breathing trajectories scaled to 4 cm amplitude peak-to-peak motion with a corresponding 4 cm s^{-1} peak velocity. Coronal CT images of the static and moving sponge are shown in Figure 2. An abdominal bellows system (Philips Medical Systems, Cleveland, OH) was attached to a synchronized motion stage and used to provide a breathing cycle surrogate. The bellows voltage signal was sampled at 100 Hz, using a PC with analog-to-digital converter controlled using custom LabVIEW software (National Instruments, Austin, TX). Signals were analysed further using Matlab software (v. R2013a; Mathworks, Natick, MA). The phantom was scanned whilst static, Figure 2a, and during "free-breathing", Figure 2b, using a 16-slice Philips Brilliance Big Bore scanner (Philips Medical Systems, Cleveland, OH), in alternating directions. Different patient breathing waveforms were applied to observe the presence of artefacts. In order to test the effect of varying directions of breathing motion with respect to scan direction, images were acquired with table motion travelling in alternating directions. Detector configuration of 12 mm, rotation period 0.44 s and helical pitch of 1.184 were used (listed in Table 2). Figure 2b shows the artefacts which arose owing to the breathing motion being greater than the scan speed. The breathing trajectory is also shown, with position and velocity displayed. The X-ray on signal from the scanner was monitored in order to synchronize the bellows signal with the images. This signal identified when the scanner was acquiring projection data and was synchronized with the DICOM (Digital Imaging and Communication in Medicine) image time tags to correct for the time when projections were acquired. The bellows voltage signals were smoothed using a central moving average filter, and the rate of signal change was calculated (V/s) to give a surrogate measurement of tissue velocity.

Patient data

Five patients were enrolled under an IRB protocol and scanned using either a 16- (one patient) or 64-slice scanner (five patients), with the scan settings listed in Table 2. The bellows was wrapped around the patient's abdomen to record breathing amplitude. Figure 1a shows a free-breathing image acquired using a 64-slice scanner. Images were acquired with a detector configuration (longitudinal field of view) of 38.4 mm, pitch of 1.2 and scanner rotation period of 0.285 s which resulted in a table movement of 46.08 mm per rotation and a table velocity of 161.7 mm s^{-1}. The scans used 120 kV and 40 effective mAs per slice (169 mA for this pitch and rotation time). Images were reconstructed with 1-mm

Figure 2. Scans of the sponge phantom using the 16-slice Philips Brilliance Big Bore CT scanner. (a, d) Static scan of the sponge. (b, e) Two different breathing trajectories (4 cm peak–peak amplitude, position shown with thin line, velocity with thick line) are applied to the sponge, and artefacts are present at regions of maximum motion velocity (artefacts encircled). (c, f) Simulation of scan shown in (b, e) with similar artefacts arising owing to motion. The static scan is shown next to each dynamic image to show the image distortion caused by motion.

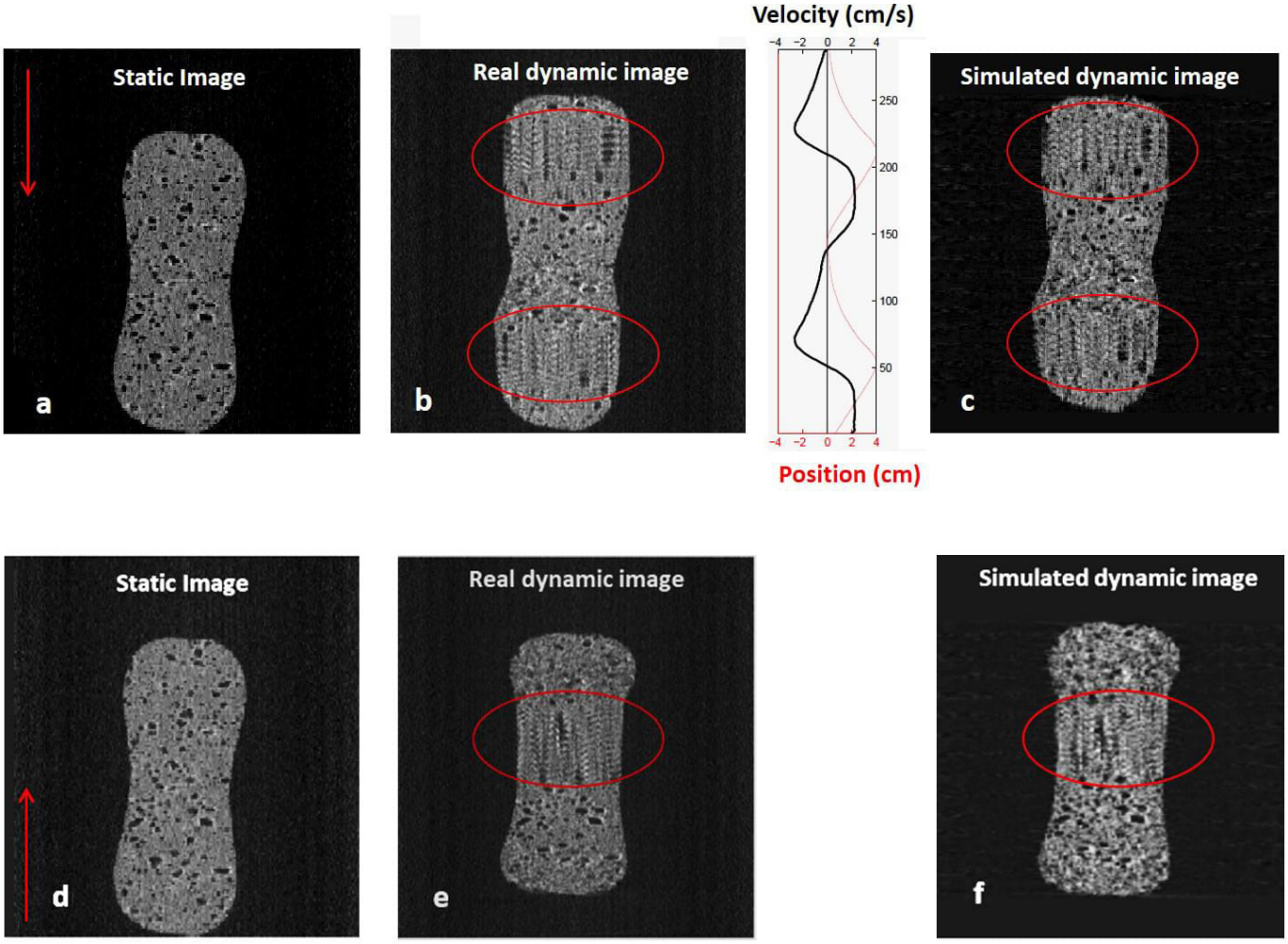

slice thickness using the Siemens reconstruction kernel B30f. This protocol required approximately 2.5 s to scan the entire lung volume from apices to lung bases, for a typical patient. The entire scanning sequence took approximately 140 s. The total $CTDI_{vol}$ for the entire scan (all 25 acquisitions) was 4.22 cGy, which is less than a current clinical slow-helical 4D-CT protocol (Siemens Sensation Open, 800 mAs, spiral pitch of 0.1, $CTDI_{vol}$ of 6.9 cGy). Although images were distorted owing to breathing motion (images do not correspond to any single breathing phase), they were free of motion-induced artefacts which would affect accurate image registration. Figure 1b shows a free-breathing image acquired using a 16-slice scanner. Images acquired using the slower 16-slice scan parameters took approximately 4 s to scan 30 cm. The image shown in Figure 1b was acquired during the maximum diaphragm velocity. The diaphragm motion caused motion artefacts owing to the inconsistencies of the measured X-ray projections and their subsequent use in the image reconstruction process.

RESULTS

Phantom data (16 slice)

Figure 2 shows a coronal slice from (a,d) the static image of the phantom scanned in opposite directions. Figure 2b,e shows the real dynamic scans and two of the breathing trajectories that were applied to the phantom in each case. Scan direction is shown with arrows in (a, d). The breathing trajectory relative to the scan direction applied in (b) caused the image of the sponge to be elongated, with two regions of motion artefacts present at negative breathing velocity (same direction as the scanner); the sponge appears to be "stretched" in this region, as the same region of the phantom is being acquired in multiple image slices. The breathing trajectory applied in (d) caused the image of the sponge to be shortened overall, owing to the opposite direction of breathing motion to the scan direction, although a single region of doubling motion artefacts is present at positive breathing velocity (same direction as the scanner). Artefacts of this type were found when all of the five patient waveforms were applied to the phantom. The static

Figure 3. Simulated 16-mm detector configuration (a–f, rotation time 0.1–0.6 s) and 64-mm detector configuration (g-l, rotation time 0.2–2.0 s) images. Artefacts have been identified visually (circles). Increasing amounts and severity of artefacts are present in the images for increasing rotation times. Doubling artefacts were present in 16-mm detector configuration images >0.1 s rotation time. Blurring artefacts were present in 64-mm detector configuration images with rotation time >0.8 s.

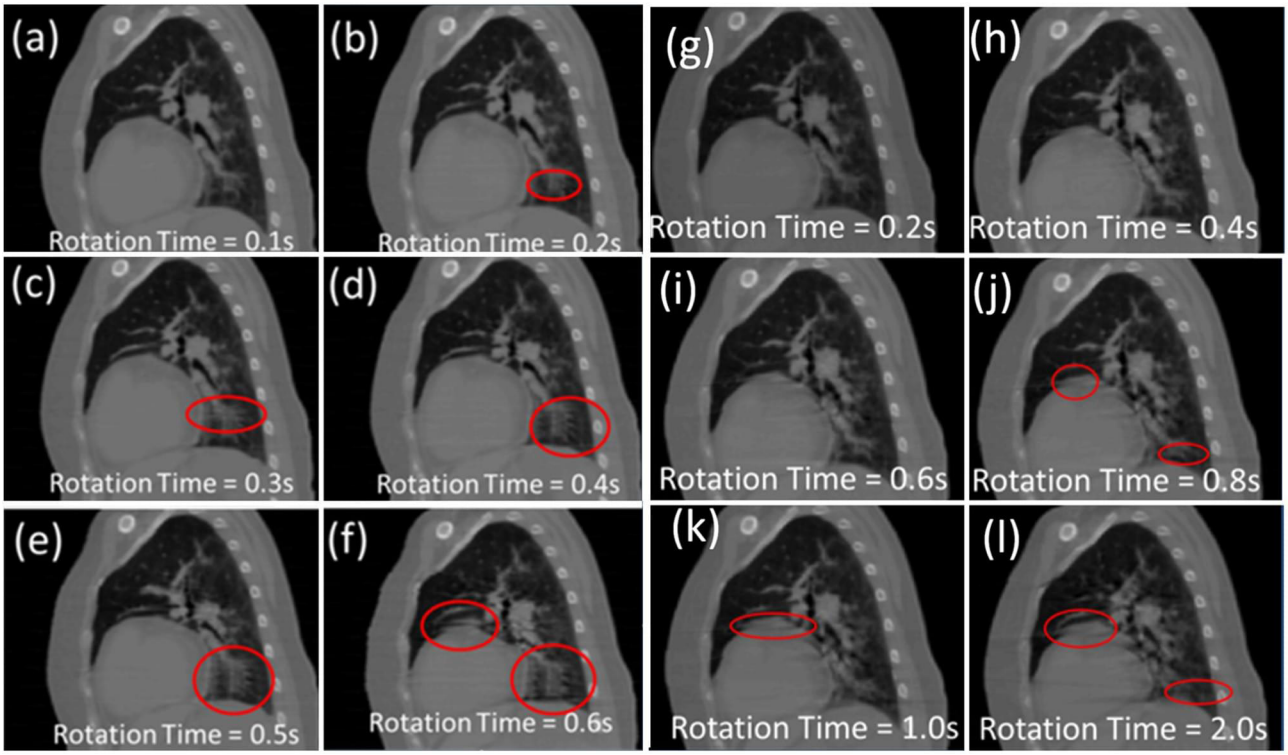

scans (a, d) are identical in both directions and contain no motion artefacts. Figure 2c,e shows the simulated versions of each of the dynamic images. The simulated images (d, f) closely matched the real images (b, e), confirming that the scanner simulation yielded realistic motion-induced artefacts. A slight offset existed between the real and simulated scans caused by differences in the start times with respect to the breathing trajectory, owing to limitations in the X-ray to bellows synchronization process. The presence of artefacts was not affected by these offsets. Attempts to recover the phantom motion trajectories using DIR were unsuccessful owing to the severity of the doubling artefacts in both images. The 64-slice equivalent images contained no such motion artefacts with the breathing trajectories applied, owing to the increased scan speed.

Patient data

Figure 3 (left columns) shows examples of images generated using a simulated 16-mm detector configuration, with gantry rotation time varying from (a) 0.1 s per rotation to (f) 0.6 s per rotation (sagittal image slices in the left lung shown). Distinct artefacts are encircled. For rotation times greater than 0.1 s per rotation, doubling artefacts were present, and vessels in the bottom and the back of the lung appeared more than once in the images. The severity and coverage of these artefacts increased with increasing rotations times, and for rotation times greater than 0.5 s similar artefacts were also visible above the heart.

Figure 4 shows the SSM maps of the images in Figure 3, showing an increase in SSM in the regions corresponding to the visible artefacts. A threshold value of SSM >0.7 was found to correlate to obvious doubling artefacts. The percentage of the image area with SSM > 0.7 is shown in Figure 5 with the artefact area plotted against rotation time. The right columns of Figures 3 and 4 show the examples of 64-slice images, infer that the 64-slice images have fewer motion-induced artefacts than the 16-slice scan images owing to the faster scan speeds. When comparing the SSM maps for the 64-slice images, no trend was observed as a function rotation time up to the maximum evaluated tim e of 2.0 s. There were some motion blurring artefacts, encircled in Figure 3.

DISCUSSION

Increasing amounts of doubling-artefacts were observed with increasing rotation times > 0.2 s for 16 mm slice scan geometry. Quantifying artefacts by comparing to "ground-truth" images is not possible here, as the doubling artefacts are owing to the presence of real tissue being imaged twice. Here, SSM was used as a quantitative measure of doubling artefacts, validated by visually inspecting the images. Figures 4 and 5 show that using a 16-mm detector configuration, a rotation time of less than or equal to 0.2 s (53 mm s^{-1} scan speed) would be required to produce images of similar quality to those acquired using the simulated 64 mm slice scan geometry. While only the effect of decreasing the rotation speed has been investigated here, a similar effect

Figure 4. Structural similarity metric (SSM) maps calculated slice-by-slice for the 16- (a–f, rotation time 0.1–0.6 s) and 64-mm detector configuration (g–l, rotation time 0.2–2.0 s) segmented lung images shown in Figure 3. The SSM maps show increasing amounts of structural similarity between axial slices, corresponding to increased doubling artefacts with increasing rotation time in the 16-mm detector configuration images. No significant increase in SSM is observed for the 64-mm detector configuration data.

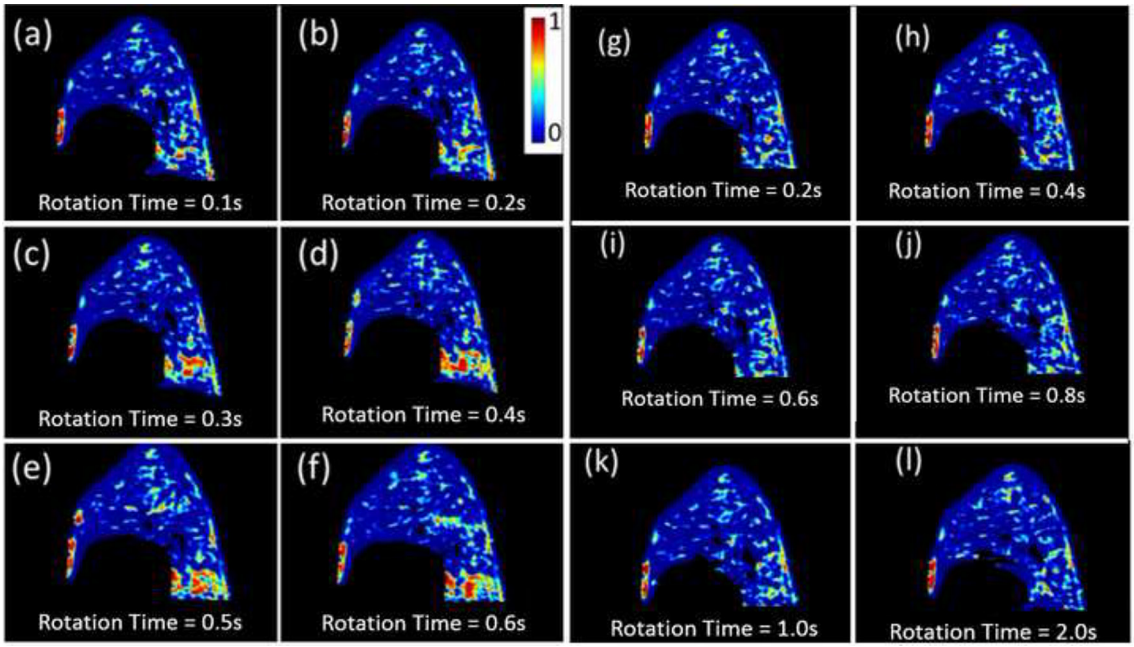

could be achieved by increasing the nominal slice widths of the detector, as shown by Tanyi et al.[14]

If tissue motion is greater than and in the same direction as the CT scan acquisition, individual vessels may appear more than once in a single scan. If the motion is in the opposite direction, the projections of the vessel will be incomplete, and the vessel may be missing entirely from the reconstructed image. These artefacts will cause the image reconstruction to be challenging. 5DCT techniques based on image registration of free-breathing fast-helical CT images require the images to be deformed by breathing motion, but artefact-free in order for DIR software to adequately estimate the motion between such free-breathing images. If the CT scanning speed is much less than the tissue motion of interest, the blurring and doubling artefacts shown in the presented data will reduce the registration and ultimately the motion model accuracy, limiting the usefulness of images or other motion analysis generated using the model.

Figure 5. Graph shows the percentage of image area identified as doubling-artefact (SSM > 0.7) as a function of rotation time (0.1–0.6 s), for 16- and 64-slice images. SSM, structural similarity metric.

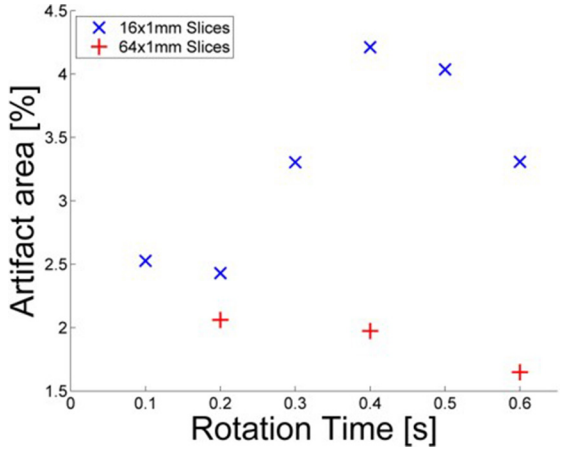

Phantom data were presented here for two reasons. Firstly, to test images for the presence of artefacts when realistic breathing trajectories were applied, which were observed in all of the five patient breathing trajectories tested here, and secondly to test the ability of the scanner simulation to successfully predict these. Phantom data alone provided information on the presence of artefacts at known tissue velocity thresholds. The phantom motion used here was a simple one dimensional trajectory approximation using a range of velocities. As shown in Figure 2, the type, severity and location of such artefacts have a complex relation to the breathing and scan velocities. Conclusions made from phantom data alone may be incomplete, and would not take into account three dimensional tissue motions.

As it is not feasible to do an exhaustive test of scanning parameters using real patients owing to the radiation dose that would be delivered, the five patient scanner simulation presented here provided a more realistic simulation to the process of scanning real patients using the published 5DCT protocol. The choice of scanning parameters on commercial CT scanners are limited

owing to restrictions such as tube current limitations or maximum gantry speed limits, whereas the simulations presented here were subject to no such constraints, and we were able to offer useful information to guide the specifications of the next generation of CT scanner designed to support the 5DCT protocol.

One limitation of the scanner simulation was the simplicity of the forward projection calculations. Although there are three general components to a projection image, namely primary signal, scatter signal and noise signal,[21] we considered only the primary signal here, which characterized the photon attenuation. We assumed that the signal-to-noise ratio of the images was sufficiently large that variations in scatter and noise with breathing motion would not significantly impact the conclusions.

CONCLUSION

The current generation of 16-slice CT scanners, which are present in the majority of Radiation Oncology departments, are not capable of generating free-breathing sorting artefact-free images in the majority of patients.

FUNDING

This work was supported by NIH R01 CA0096679. The NVIDIA Quardro K1200 GPU used for this research was donated by the NVIDIA Corporation.

REFERENCES

1. Kyriakou E, McKenzie DR. Changes in lung tumor shape during respiration. *Phys Med Biol* 2012; **57**: 919–35. doi: https://doi.org/10.1088/0031-9155/57/4/919
2. Keall PJ, Mageras GS, Balter JM, Emery RS, Forster KM, Jiang SB, et al. The management of respiratory motion in radiation oncology report of AAPM task group 76. *Med Phys* 2006; **33**: 3874–900. doi: https://doi.org/10.1118/1.2349696
3. Bortfeld T, Jiang SB, Rietzel E. Effects of motion on the total dose distribution. *Semin Radiat Oncol* 2004; **14**: 41–51. doi: https://doi.org/10.1053/j.semradonc.2003.10.011
4. Ford EC, Mageras GS, Yorke E, Ling CC. Respiration-correlated spiral CT: a method of measuring respiratory-induced anatomic motion for radiation treatment planning. *Med Phys* 2003; **30**: 88–97. doi: https://doi.org/10.1118/1.1531177
5. Pan T. Comparison of helical and cine acquisitions for 4D-CT imaging with multislice CT. *Med Phys* 2005; **32**: 627–34. doi: https://doi.org/10.1118/1.1855013
6. Langner UW, Keall PJ. Prospective displacement and velocity-based cine 4D CT. *Med Phys* 2008; **35**: 4501–12. doi: https://doi.org/10.1118/1.2977539
7. Lu W, Parikh PJ, Hubenschmidt JP, Bradley JD, Low DA. A comparison between amplitude sorting and phase-angle sorting using external respiratory measurement for 4D CT. *Med Phys* 2006; **33**: 2964–74. doi: https://doi.org/10.1118/1.2219772
8. Abdelnour AF, Nehmeh SA, Pan T, Humm JL, Vernon P, Schöder H, et al. Phase and amplitude binning for 4D-CT imaging. *Phys Med Biol* 2007; **52**: 3515–29. doi: https://doi.org/10.1088/0031-9155/52/12/012
9. Santoro JP, Yorke E, Goodman KA, Mageras GS. From phase-based to displacement-based gating: a software tool to facilitate respiration-gated radiation treatment. *J Appl Clin Med Phys* 2009; **10**: 2982–. doi: https://doi.org/10.1120/jacmp.v10i4.2982
10. Wink N, Panknin C, Solberg TD. Phase versus amplitude sorting of 4D-CT data. *J Appl Clin Med Phys* 2006; **7**: 77–85. doi: https://doi.org/10.1120/jacmp.v7i1.2198
11. Chen GT, Kung JH, Beaudette KP. Artifacts in computed tomography scanning of moving objects. *Semin Radiat Oncol* 2004; **14**: 19–26. doi: https://doi.org/10.1053/j.semradonc.2003.10.004
12. Sarker J, Chu A, Mui K, Wolfgang JA, Hirsch AE, Chen GT, et al. Variations in tumor size and position due to irregular breathing in 4D-CT: a simulation study. *Med Phys* 2010; **37**: 1254–60. doi: https://doi.org/10.1118/1.3298007
13. Thomas D, Lamb J, White B, Jani S, Gaudio S, Lee P, et al. A novel fast helical 4D-CT acquisition technique to generate low-noise sorting artifact-free images at user-selected breathing phases. *Int J Radiat Oncol Biol Phys* 2014; **89**: 191–8. doi: https://doi.org/10.1016/j.ijrobp.2014.01.016
14. Tanyi JA, Fuss M, Varchena V, Lancaster JL, Salter BJ. Phantom investigation of 3D motion-dependent volume aliasing during CT simulation for radiation therapy planning. *Radiat Oncol* 2007; **2**: 10. doi: https://doi.org/10.1186/1748-717X-2-10
15. Delmon V, Rit S, Pinho R, Sarrut D. Registration of sliding objects using direction dependent B-splines decomposition. *Phys Med Biol* 2013; **58**: 1303–14. doi: https://doi.org/10.1088/0031-9155/58/5/1303
16. Low DA, White BM, Lee PP, Thomas DH, Gaudio S, Jani SS, et al. A novel CT acquisition and analysis technique for breathing motion modeling. *Phys Med Biol* 2013; **58**: L31–9155L36. doi: https://doi.org/10.1088/0031-9155/58/11/L31
17. Katsevich A. An improved exact filtered backprojection algorithm for spiral computed tomography. *Adv Appl Math* 2004; **32**: 681–97. doi: https://doi.org/10.1016/S0196-8858(03)00099-X
18. Tan J, Li HH, Klein E, Li H, Parikh P, Yang D, et al. Physical phantom studies of helical cone-beam CT with exact reconstruction. *Med Phys* 2012; **39**: 4695–704. doi: https://doi.org/10.1118/1.4736535
19. Wang Z, Bovik AC, Sheikh HR, Simoncelli EP, Zhou W. Image quality assessment: from error visibility to structural similarity. *IEEE Trans Image Process* 2004; **13**: 600–12.
20. Wu G, Wang Q, Lian J, Shen D. Estimating the 4D respiratory lung motion by spatiotemporal registration and super-resolution image reconstruction. *Med Phys* 2013; **40**: 031710. doi: https://doi.org/10.1118/1.4790689
21. Jia X, Yan H, Cervino L, Folkerts M, Jiang SB. A GPU tool for efficient, accurate, and realistic simulation of cone beam CT projections. *Med Phys* 2012; **39**: 7368–78. doi: https://doi.org/10.1118/1.4766436